Applied Thermal Engineering 211 (2022) 118445

Contents lists available at ScienceDirect

Applied Thermal Engineering

journal homepage: www.elsevier.com/locate/apthermeng

Research Paper

Optimization of the pitch to chord ratio for a cascade turbine blade in wet steam flow

Mohammad Reza Aghdasi [a], Ali Reza Teymourtash [a,*], Esmail Lakzian [b,c]

[a] Department of Mechanical Engineering, Ferdowsi University of Mashhad, Mashhad, Iran
[b] Center of Computational Energy, Department of Mechanical Engineering, Hakim Sabzevari University, Sabzevar, Iran
[c] Peoples' Friendship University of Russia (RUDN University), 6 Miklukho-Maklaya Street, 117198 Moscow, Russian Federation, Russia

ARTICLE INFO

Keywords:
Wet steam flow
Optimization
Zweifel coefficient
Pitch to chord ratio
Wetness fraction
Isentropic efficiency

ABSTRACT

This study has used shape optimization by the genetic algorithm to gain the suitable pitch to axial chord ratio for a cascade turbine blade. The innovation of the present paper is the modification of the Zweifel coefficient for the wet steam flow passing through the steam turbine cascade. Wetness fraction (WF), average droplet radius (ADR), momentum (MO), pressure loss (PL), and isentropic efficiency (IE) at the exit of the cascade turbine blade in wet steam flow are selected as the objective functions. The ultimate goal was to minimize the wetness fraction, average droplet radius at the outlet of the blade, and pressure losses of the passage and maximize the efficiency and momentum at the outlet together. The Navier-Stokes equations,S*STk* $-\omega$ turbulence model, and the Eulerian-Eulerian approach are applied for modeling the condensing flow. The agreement gained between the numerical results and the experimental results is satisfactory. A pitch to axial chord ratio of Pi/AC = 0.76 is suggested, and the modified Zweifel coefficient for wet steam flow in the cascade is proposed $C_{ZF} = 0.62$. In the optimal case, the wetness fraction and the average droplet radius at the outlet decrease 3.59% and 1.94%, respectively, and the momentum increases 7.28%. In addition, the optimal case compares with original case, the isentropic efficiency decreases 2.48% and the pressure losses increases 2.15%.

1. Introduction

Finding the optimal pitch to chord ratio of steam turbines has been a challenging task ever since because it has an essential effect on efficiency and losses. In addition, the last stages of the steam turbine are associated with condensation. This phenomenon leads to the attendance of a liquid phase which results in thermodynamic and mechanical losses. It should be noted if the wetness fraction is increased by one percent, the efficiency will decrease as well [1]. Therefore, the perception of the condensation phenomenon is greatly useful in the design process. A plethora of studies are conducted on the phenomenon of condensation. Dykas et al. [2] evaluated the non-equilibrium condensing steam flow of transonic in half arc nozzles and stator blades which were located in the last stage of the steam turbine. Dykas et al. [3] experimentally investigated the condensation of steam flows in a non-equilibrium state which occurred in a linear rotor blades cascade. Their studies goal to prepared an experimental data for validation of the numerical methods in the wet steam flow. Walker et al. [4] reviewed the various techniques to measure the wetness content including the liquid film and moisture content. Joseph et al. [5] described a numerical approach to calculate the thermodynamic loss related to non-equilibrium condensation for the nozzle and turbine cascade. The thermodynamic loss was calculated utilizing the variation in entropy owing to condensation. Wróblewski and Dykas [6] presented a model intended for the condensing steam flow through the de Laval nozzle to reconstruct the size of a water droplet. Results illustrated a better agreement for suggested model with an experimental data on the static pressure distributions. Cao et al. [7] indicated that parameters of flow field and location of vortex impressed the droplet size, number of droplets, and condensation location of the steam turbine. The energy losses due to rotor blade profile and droplet size were studied by Sengupta and Bhattacharya [8]. Salmani et al. [9] proposed an innovative method to predict droplet radius and wetness fraction regarding roughness in the turbine blades. Their method was founded on Buckingham Pi-theorem and merely the use of dry vapor data.

Today, various methods have been stated to reduce the wetness and losses in steam turbines and nozzles. Fizik et al. [10] studied the effects of variation in the rate of expansion and the divergent angle of a turbine blade. They obtained suitable conditions with minimum thermodynamic losses by the criterion of entropy generation. Alekseev et al. [11]

* Corresponding author.
E-mail address: teymourtash@um.ac.ir (A.R. Teymourtash).

https://doi.org/10.1016/j.applthermaleng.2022.118445
Received 6 November 2021; Received in revised form 3 March 2022; Accepted 29 March 2022
Available online 31 March 2022

Nomenclature

A	area
AC	axial chord
ADR	average of droplet radius
ADRR	average of droplet radius ratio
B_2, B_3	virial coefficients
C	velocity magnitude
C_x, C_y, C_z	velocity components
C_S	isentropic velocity
C_{ZF}	Zweifel's coefficient
C_l	specific heat of liquid
C_p	specific heat at constant pressure
C_v	specific heat at constant volume
e_0	total energy
G	Gibbs free energy
h_0	total enthalpy
I	droplet nucleation rate
IE	isentropic efficiency
IER	isentropic efficiency ratio
K_b	Boltzmann's constant
K_t	thermal conductivity
k	turbulence kinetic energy
m_r	liquid mass
M_m	molecular mass
MO	momentum at outlet
MOR	momentum ratio
P	pressure
Pi	pitch
PL	pressure losses
PLR	pressure losses ratio
q_c	condensation coefficient
R	gas constant
r	droplet radius
$\bar{r}$	average radius
S	supersaturation ratio
T	temperature
t	time
V_d	average volume of droplet
$\overline{w}$	average wetness fraction
WF	wetness fraction
WFR	wetness fraction ratio
x	axial length of the blade
x, y, z	cartesian directions

Greek letters

α_1, α_2	inlet and outlet angles
β	liquid mass fraction
Γ	mass generation rate
η	number of droplets per volume
ρ	density
τ	viscous stress tensor
μ	dynamic viscosity
σ	liquid surface tension

Subscript

d	droplet
g	gas
i	isentropic
l	liquid
lv	liquid–vapor
mix	mixture (liquid–vapor)
s	saturation
v	vapor

Superscript

*	critical

presented the experimental results of the impact of intra-channel liquid film suction of the wet steam turbine blade. Their results demonstrated that the number of droplets was decreased by this method. Fizik et al. [12] numerically investigated the effect of the attendance of wetness at the inlet of stationary turbine blade cascades. Their results demonstrated that attendance of moisture at inlet significantly reduced the supercooling degree and nucleation process was delayed. Ding et al. [13] studied the impact of surface roughness and operation back pressure of condensing steam flow on entropy generation and exergy destruction in turbine blades. Their results indicated that turbulent viscosity and intermittency were influenced significantly by roughness. Based on their results, by increasing the average height of roughness, the total entropy generation and exergy destruction were increased as well. Zhang et al. [14] optimized the structure of novel dehumidification to decrease the wetness loss and improve the efficiency of a steam turbine.

The injection is one of the most challenging methods in which the researchers are interested. Aliabadi et al. [15] investigated the water spray injection at the inlet of the turbine blade cascade to control the two-phase heat transfer. Their results showed that the total two-phase heat transfer and condensation losses were reduced by droplet injection. Also, Aliabadi et al. [16] utilized hot steam injection to reduce the rate of erosion and condensation loss. Their results indicated that by injecting hot steam, blade corrosion rate and condensation loss were reduced due to the reduction of droplets. Mirhoseini and Boroomand [17] assessed the effect of hot steam injection on converging–diverging nozzles. The genetic algorithm approach for multi-objective optimization was utilized to obtain suitable injection values.

Volumetric heating is a common method for decreasing the losses of the wet steam turbine. Vatanmakan et al. [18] evaluated the impacts of various rates of volumetric heating on wetness fraction and entropy generation in steam turbine cascade. They proposed appropriate volumetric heating which reduced the corrosion and entropy generation. Hosseini and Lakzian [19] introduced a method to optimize the volumetric heating which was applied to the converging section of the steam turbine. Reduction of entropy losses, economic cost, and wetness were the objectives of their optimization. Hosseinzade et al. [20] utilized a genetic algorithm to optimize volumetric heating for the steam turbines; the optimal volumetric heating for the reduction of the wetness was provided at the end of the study.

Researchers are interested in reducing the losses through shape optimization. The last stage of a 100 Hz industrial gas turbine blade was optimized by Sui et al. [21]. The parameters of their study were the number of blades and axial chord to blade height. They suggested a fewer blades number with longer cord for designing the last stage blade to gain higher efficiency and good strength. Mahrooghi and Lakzian [22] illustrated that the performance of Wells turbines can be substantially enhanced by adding guide vanes, endplate, or end ring to the base blade. The proposed blade improved the efficiency and torque coefficient and decreased the pressure drop coefficient. Trigg et al. [23] utilized GA to propose a systematic approach for obtaining optimal blade profile with minimum losses. Keisari and Shams [24] utilized the genetic algorithm to optimize the shape of the wet-steam nozzle. Their results showed that the size and number of droplets were improved by 5.61% and 10.7%, respectively. Yang et al. [25] investigated the impact of the trailing edge cutback on the performance of the blade. They suggested the 14% cutback of the trailing edge which improved the blade performance. Rahimabadi et al. [26] used the genetic algorithm approach to shape the optimization of turbine blades. Maximum droplet radius and

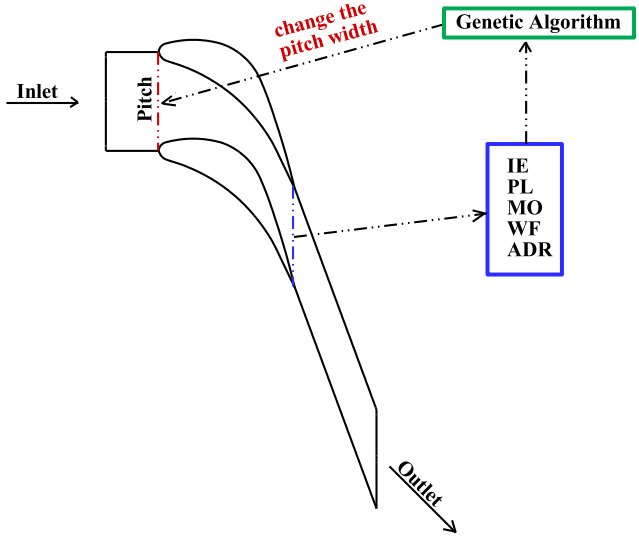

Fig. 1. Schematic illustration of the turbine blade, flow passage, optimization loop based on the change in the pitch width, and objective function at the end of the passage.

Table 1
Geometrical specifications for the turbine blade cascade [37].

Chord	Pitch	Axial chord	Inlet flow angle
35.76 mm	18.26 mm	25.27 mm	0^0

Table 2
Boundary conditions of turbine cascade blade [38].

$\mathbf{P}_{0_{in}}$	172 kPa
$\mathbf{T}_{0_{in}} = \mathbf{T}_s(\mathbf{P}_{0_{in}}) - 8$	380.66 K
$\mathbf{P}_{out} = 0.48\mathbf{P}_{0_{in}}$	82.56 kPa

rate of droplet nucleation were the objectives of this optimization. Their results demonstrated that their method improved the turbine blade efficiency up to 2.1%. Han et al. [27] studied the effects of the non-axisymmetric end wall of the turbine blade cascade on steam parameters. Their results indicated that the non-axisymmetric end wall decreased the droplet size.

In the design of the steam turbine, the optimization of the ratio of pitch to chord for blades is one of the most essential concerns of researches. Zweifel [28] in an experimental study, proposed the optimal ratio of pitch to chord for dry steam turbine blades and showed the effect of pitch changes on the magnitude of losses. Dossena and D'Ippolito [29] investigated the effect of three incidence angles, six Mach numbers, and three pitch to chord ratios, on the development of secondary flows of turbine cascades. Their results indicated that stagger angle and pitch to chord ratio caused wide impacts on the cascade losses. Walker and Hesketh [30] optimized the low-reaction steam turbine blades by changing the pitch to chord ratio. Results showed that if the blades are spaced well apart, the profile losses will decrease, but, the secondary loss will increase. Segawa and Shikano [31] proposed an optimal reaction blade of a steam turbine that operates on a high-pressure condition. Pitch to chord ratio, a radius of leading-edge, turning angle and maximum blade loading location were the control factors of that study. Results denoted that stage efficiency was increased by about 1.5% with an optimum blade. A highly loaded rotor cascade, which had an increase of pitch to chord ratio by 14% without deterioration of performance, has been developed by Segawa and Shikano [32]. Teia [33] suggested a new supersonic loss model to produce a more efficient design of a compact turbine. Their results illustrated that pitch to chord ratio had a significant effect on the shock system. Mesbah et al. [34] evaluated the effect of geometric parameters involving, the blade aspect ratio and pitch-to-chord ratio in a stator cascade of an axial turbine. Their results showed that as the pitch-to-chord ratio increased from 0.7 to 0.75, the total energy losses were reduced by 12.2 %. Then by increasing the pitch-to-chord ratio from 0.75 to 0.8, the total energy losses increased by 6 %. Flidr et al. [35] evaluated the kinetic energy loss and the secondary loss in two cascades with different pitch to chord ratio (t/c = 0.6 and 0.9), respectively. Lengani et al. [36] investigated the proper orthogonal decomposition (POD) which had been applied to a large dataset explaining the profile losses of low-pressure turbine. They used two cascades with two Zweifel numbers. Their results could be beneficial to decrease the number of simulations.

To the best of our knowledge, no attempt was reported to optimize the pitch to axial chord ratio in turbine blade cascade in wet steam flow based on (wetness fraction (WF), average droplet radius (ADR), momentum (MO), pressure loss (PL), and an isentropic efficiency (IE)) and Zweifel's criteria. Therefore, in this study, the effects of variations of the pitch to axial chord ratio in turbine blade cascade in wet steam flow are studied. The innovation of the present study is the modification of the Zweifel coefficient for the wet steam flow passing through the steam turbine cascade. In this regard, The Navier-Stokes equations,$SSTk-\omega$ turbulence model, and the Eulerian-Eulerian approach are applied for modeling the condensing flow. In addition, a multi-objective method is used for the optimization process. For this purpose, wetness fraction (WF), average droplet radius (ADR), momentum (MO), pressure loss (PL), and an isentropic efficiency (IE), all calculated at the exit of the blade, are introduced as a criterion for proposing the optimal cases. Moreover, Fig. 1 shows the schematic of the present study.

2. Introducing geometry and boundary conditions

In the present study, the nozzle blade of Bakhtar et al. [37] is used. In addition, more information about this cascade is presented in the Table 1.

The boundary conditions are expressed in Table 2. Pressure type is considered for inlet and outlet boundary, and blades' sides are fixed and followed by no-slip conditions. The periodic boundary conditions are also utilized at the inlet and outlet of the passage. Fig. 2 illustrates the geometry and boundary conditions.

3. Governing equations

The Eulerian-Eulerian approach is employed to model the condensing steam flow. The two-phase flow is simulated utilizing the two-dimensional viscous compressible Navier-Stokes equations and energy equation, combined with nucleation and the droplet growth equations.

3.1. Conservation equations

Conservation equations of mass, momentum, and energy for viscous compressible condensing steam flow in two-dimensional cartesian coordinates can be written as follows [39]:

$$\frac{\partial W}{\partial t}+\frac{\partial F}{\partial x}+\frac{\partial G}{\partial y}=\frac{\partial R}{\partial x}+\frac{\partial S}{\partial y} \tag{1}$$

In the above-mentioned equations, W shows the independent variable vector, F and G indicate non-viscous terms, S and R denote viscous terms as shown:

$$W=\begin{bmatrix}\rho\\ \rho C_x\\ \rho C_y\\ \rho e_0\end{bmatrix}, F=\begin{bmatrix}\rho C_x\\ P+\rho {C_x}^2\\ \rho C_x C_y\\ \rho C_x h_0\end{bmatrix}, G=\begin{bmatrix}\rho C_y\\ \rho C_y C_x\\ P+\rho {C_y}^2\\ \rho C_y h_0\end{bmatrix}$$

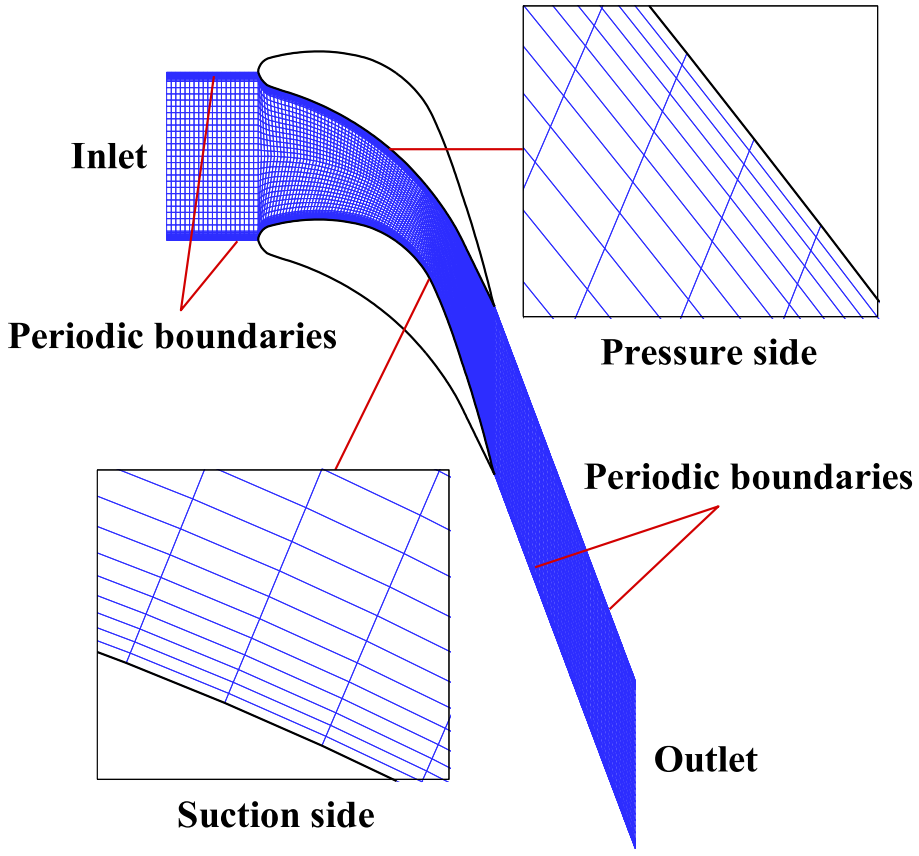

Fig. 2. Computational grid and the boundary conditions of the cascade turbine blade.

$$S=\begin{bmatrix}0\\ \tau_{xy}\\ \sigma_y\\ \sigma_y C_y+\tau_{xy}C_x+k\dfrac{\partial T}{\partial y}\end{bmatrix}, R=\begin{bmatrix}0\\ \sigma_x\\ \tau_{yx}\\ \sigma_x C_x+\tau_{yx}C_y+K_t\dfrac{\partial T}{\partial x}\end{bmatrix} \tag{2}$$

In the above expressions, P, ρ, K_t C_x, C_y, e_0, and h_0 represent pressure, density, heat transfer coefficient, velocity components in × and y directions, total energy, and total enthalpy, respectively.

$$e_0 = e+\frac{C^2}{2} \tag{3}$$

$$h_0 = h+\frac{C^2}{2} \tag{4}$$

$$C^2 = C_x^2+C_y^2 \tag{5}$$

In addition, σ_x, σ_y are normal stress, and τ_{yx}, τ_{xy} are shear stress as:

$$\sigma_x = -\frac{2}{3}\mu_{eff}\left(\frac{\partial C_x}{\partial x}+\frac{\partial C_y}{\partial y}\right)+2\mu_{eff}\frac{\partial C_x}{\partial x} \tag{6}$$

$$\sigma_y = -\frac{2}{3}\mu_{eff}\left(\frac{\partial C_x}{\partial x}+\frac{\partial C_y}{\partial y}\right)+2\mu_{eff}\frac{\partial C_y}{\partial x} \tag{7}$$

$$\tau_{xy}=\tau_{yx}=\mu_{eff}\left(\frac{\partial C_x}{\partial y}+\frac{\partial C_y}{\partial x}\right) \tag{8}$$

Effective viscosity (μ_{eff}) is the sum of turbulent viscosity (μ_t) and molecular viscosity (μ). It is worth mentioning that two-phase density is based on the liquid phase and vapor phase and is calculated as follows in which β is the liquid mass fraction.

$$\rho=\frac{\rho_v}{1-\beta} \tag{9}$$

It should be noted that the conservation equations are calculated with respect to the properties of the two-phase mixture as [40]:

$$\phi_{lv}=\phi_l\beta+(1-\beta)\phi_v \tag{10}$$

here ϕ indicates properties such as entropy, enthalpy, thermal conductivity, and specific heat. In addition, liquid mass-fraction, β, and the number of droplets per unit volume, η, were solved as follows [41]:

$$\frac{\partial\rho\beta}{\partial t}+\frac{\partial}{\partial x_i}(\rho C_i\beta)=\Gamma \tag{11}$$

$$\frac{\partial\rho\eta}{\partial t}+\frac{\partial}{\partial x_i}(\rho C_i\eta)=\rho I \tag{12}$$

where Γ represents mass generation per unit volume, I denotes the rate of droplet nucleation, and ρ indicates the two-phase density. In addition, η displays the droplets number as follows:

$$\eta=\frac{\beta}{(1-\beta)V_d\left(\frac{\rho_l}{\rho_v}\right)} \tag{13}$$

where, V_d is average droplet volume. With the assumption that the droplets are spherical, V_d is expressed as follows [42]:

$$V_d=\frac{4}{3}\pi\bar{r}^3 \tag{14}$$

3.2. Nucleation and droplet growth equation

Condensation of steam flow leads to phase change phenomenon

Table 3
Constant parameters of the state equation.

τ_0	τ_1	τ_2	γ_1	γ_2	b_1	b_2	b_3	b_4	b_5
0.897	1500/T	T/647.286	10,000	11.16	0.0015	942×10^{-3}	-488.2×10^{-6}	1.722	1.5×10^{-6}

which involves nucleation and droplet growth processes. To form droplets, if the molecular clusters overcome the free critical energy obstacles, spontaneous condensation occurs. The variation of the Gibbs free energy can be written as [41]:

$$\Delta G = -m_r R T_v Ln S + 4\pi r^2 \sigma \tag{15}$$

where S shows the supersaturation ratio and it is defined as [43]:

$$S = \left(\frac{P}{P_s(T_v)}\right) \tag{16}$$

where P represents vapor pressure and $P_s(T_v)$ indicates saturation pressure at vapor temperature. According to thermodynamic equilibrium, there is a critical radius, r^*, that must be achieved to form a stable core from supercooled vapor. In addition, the variation of critical Gibb's free energy is defined as ΔG^*. In this regard, by derivatizing Eq. (15), the ΔG^* and r^* are calculated as [44]:

$$\Delta G^* = \frac{4}{3}\pi r^{*2}\sigma \tag{17}$$

$$r^* = \frac{2\sigma}{\rho_l R T_v Ln S} \tag{18}$$

The classical theory of homogeneous condensation expresses the formation rate of the liquid droplet embryos from a supersaturated steam as follows [45]:

$$I_{classic} = q_c \frac{\rho_v^2}{\rho_l}\sqrt{\frac{2\sigma}{\pi M_m^3}} exp\left(-\frac{4\pi r^{*2}\sigma}{3K_b T_v}\right) \tag{19}$$

where q_c indicates the coefficient of condensation, which is assumed to be one,K_b represents the Boltzmann constant, M_m shows the molecular mass and σ expresses liquid surface tension. A plethora of corrections have been conducted to the classical nucleation theory. Among them, Kantrowitz corrections have good enough accuracy for non-isothermal effects [39]:

$$I = \frac{1}{(1+\theta)} I_{classic} \tag{20}$$

where θ illustrates the factor of non-isothermal correction and it is defined as follows:

$$\theta = \frac{2(\gamma-1)}{(\gamma+1)}\left(\frac{h_{lv}}{RT}\right)\left(\frac{h_{lv}}{RT}-0.5\right) \tag{21}$$

where γ denotes the specific heat ratio and h_{lv} presents the enthalpy of evaporation.

Γ shows the rate of mass generation per unit volume as follows [41]:

$$\Gamma = \frac{4}{3}\pi\rho_l I r^{*3} + 4\pi\rho_l \eta \bar{r}^2 \frac{\partial \bar{r}}{\partial t} \tag{22}$$

where $\bar{r}$ indicates the average droplet radius, and $\frac{\partial \bar{r}}{\partial t}$ denotes the rate of the droplet growth:

$$\frac{\partial \bar{r}}{\partial t} = \frac{P}{h_{lv}\rho_l\sqrt{2\pi r T}}\left(\frac{\gamma+1}{2\gamma}\right) C_p(T_l - T_v) \tag{23}$$

For very small droplets ($r < 1\mu m$), Gyarmathy approximation is utilized to calculate droplet temperature T_l, in terms of vapor temperature T_v, saturation temperature T_s and droplet radius r which can be written as [44]:

$$T_l = T_s(p) - [T_s(p) - T_v]\frac{r^*}{r} \tag{24}$$

3.3. Equation of state

In the present study, the equation of state is utilized to estimate the vapor properties as follows [46]:

$$\frac{P}{\rho_v R T} = 1 + B_2\rho_v + B_3{\rho_v}^2 \tag{25}$$

here,B_2 and B_3 denote virial coefficients which are explained as:

$$B_2 = b_1\left(1+\frac{T}{\gamma_1}\right)^{-1} + b_2 \exp(\tau_1)[1-\exp(-\tau_1)]^{\frac{5}{2}}\tau_1^{-\frac{1}{2}} + b_3\tau_1 \tag{26}$$

$$B_3 = b_4(\tau_2 - \tau_0)exp(-\gamma_2\tau_2) + b_5 \tag{27}$$

In addition, other constant coefficients of the virial equation are indicated in Table 3.

3.4. Turbulence model

SST $k-\omega$ approach is used to model the turbulent wet steam flow for the turbine blade. Menter [47] investigated the effect of using this turbulent model in two regions near the wall and far from the wall. The results indicated that the mentioned model has good accuracy in the above regions. Rahimabadi et al. [26] indicated that SST k-ω in comparison with k-ε model, predicts the wet steam flow field for Moore's "Nozzle A" and Dykas's turbine blade cascade more accurately. The mentioned model includes turbulence kinetic energy k and specific dissipation rate ω, which are expressed as follows [47]:

$$\frac{\partial}{\partial t}(\rho k) + \frac{\partial}{\partial x_i}(\rho k C_i) = \frac{\partial}{\partial x_j}\left(\Gamma_k \frac{\partial k}{\partial x_j}\right) + G_K - Y_k + S_k \tag{28}$$

$$\frac{\partial}{\partial t}(\rho\omega) + \frac{\partial}{\partial x_i}(\rho\omega C_i) = \frac{\partial}{\partial x_j}\left(\Gamma_\omega \frac{\partial \omega}{\partial x_j}\right) + G_\omega - Y_\omega + D_\omega + S_\omega \tag{29}$$

where Γ_k and Γ_ω indicate the effective diffusion coefficients of k and ω. G_K denotes the turbulent kinetic energy of average velocity gradient and G_ω represents the rate of specific loss. In addition, Y_k and, Y_ω show the turbulence loss, S_ω and S_k demonstrate the specific loss rate and its source terms for turbulence kinetic energy equations, respectively, and D_ω is cross-diffusion.

3.5. Zweifel's criteria

There is an optimum pitch to chord ratio for turbine cascade blades that brings a minimum overall loss. If the pitch of the blades is selected small, the blades guide the flow greatly, but the friction losses will be high. On the other hand, with the same blades spaced well apart, friction losses are small, but, due to poor flow guidance, the losses regarding the flow separation are large. In this regard, Zweifel proposed his criterion to find the optimum pitch to chord ratio of turbine blades which is expressed as follows [28]:

$$\sigma_x.C_{ZF} = 2\frac{cos\alpha_2}{cos\alpha_1}sin(\alpha_1 - \alpha_2) \tag{30}$$

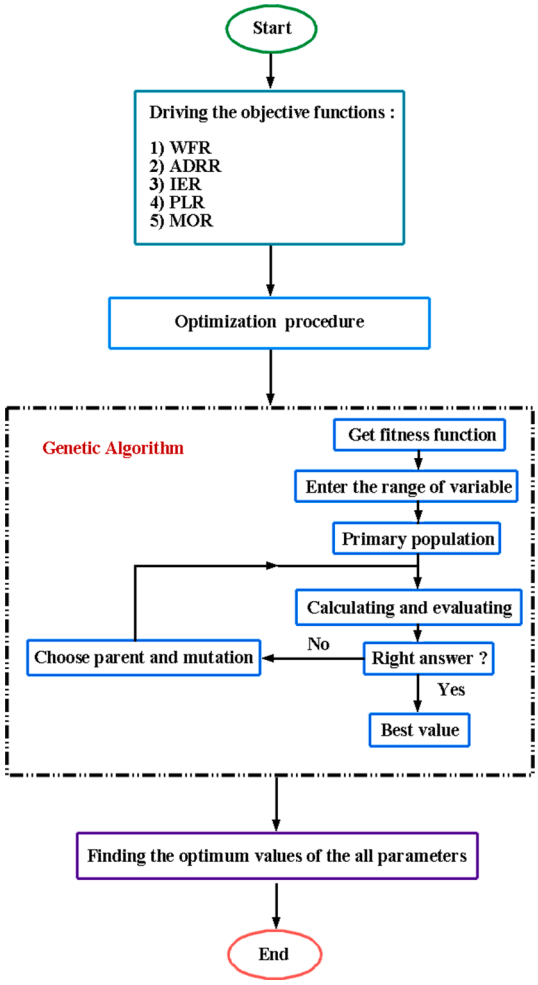

Fig. 3. Flowchart of the multi objective optimization process [49].

Table 4
Settings of the multi-objective optimization parameters.

Parameter	Value
Design variable range	[0.6, 0.88]
Maximum No. of iterations	2000
Residual error	1×10^{-6}

$$\sigma_x = \frac{Axialchord}{pitch} = \frac{AC}{Pi} \tag{31}$$

where α_1 and α_2 indicate the inlet and outlet flow angle. In addition, σ_x denotes the axial strength of the blade. Zweifel found from several experiments on turbine cascades that for minimum losses the value of C_{ZF} was approximately 0.8.

4. Multi-objective optimization

In some engineering problems, several incompatible objectives need to be discussed simultaneously. On the other hand, single-objective optimization and ignoring other objectives will yield unacceptable results [48]. In this regard, multi-objective optimization is based on an evolutionary algorithm which is a logical and perfect manner to obtain a suitable solution for the system [49]. Fig. 3 shows the flowchart of present study using the genetic algorithm method. In this paper, MATLAB software optimization toolbar has been used. According to the proposed flowchart, five objective functions including: wetness fraction rate (WFR), average droplet radius rate (ADRR), isentropic efficiency rate (IER), pressure loss rate (PLR) and momentum rate (MOR) are given to the algorithm as optimization inputs; Then, for the five stated objective functions, the five curves are fitted and the equations of the objective functions are determined. In the next step, the range of changes in the independent variable (Pi/AC) is determined and the genetic algorithm forms a population of this range. Then, according to flowchart, the algorithm processes the results. Table 4 presents the setups of the multi-objective optimization parameters of the genetic algorithm.

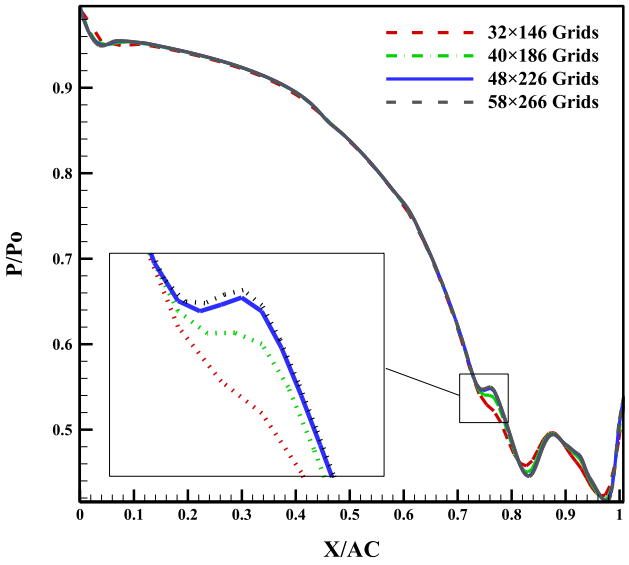

Fig. 4. Comparison of the static pressure distribution on the suction side for different grids size of the original case.

Table 5
Grid independence for different cases of the present study.

	Pitch (mm)	Pitch/Axial chord	Grid size
Case 1	15.26	0.6	40 × 226
Case 2	16.26	0.64	44 × 226
Case 3	17.26	0.68	46 × 226
Original case	18.26	0.72	48 × 226
Case 4	19.26	0.76	50 × 226
Case 5	22.26	0.88	54 × 226

4.1. Defining objective functions

Wetness fraction (WF) [50], average droplets' radius (ADR) [20], isentropic efficiency (IE) [51], pressure loss (PL) [51], and outlet momentum (MO) [51] are chosen as the objective functions of the present study. The ultimate goal is to minimize the wetness fraction, average droplet radius at the outlet of the blade, and pressure losses of the passage and maximize the efficiency and momentum at the outlet together. Next, the objective functions are explained as:

$$\mathrm{ADR} = \frac{1}{\mathrm{A}}\int_{\mathrm{A}} \overline{r}\mathrm{dA} \tag{32}$$

$$WF = \frac{1}{\mathrm{A}}\int_{\mathrm{A}} \overline{w}\mathrm{dA} \tag{33}$$

$$PL = \frac{P_{01} - P_{02}}{P_{02} - P_2} \tag{34}$$

$$IE = \frac{\int_{A2} \rho C^3 dA}{C_{2S}^2 \int_{A2} \rho c dA} \tag{35}$$

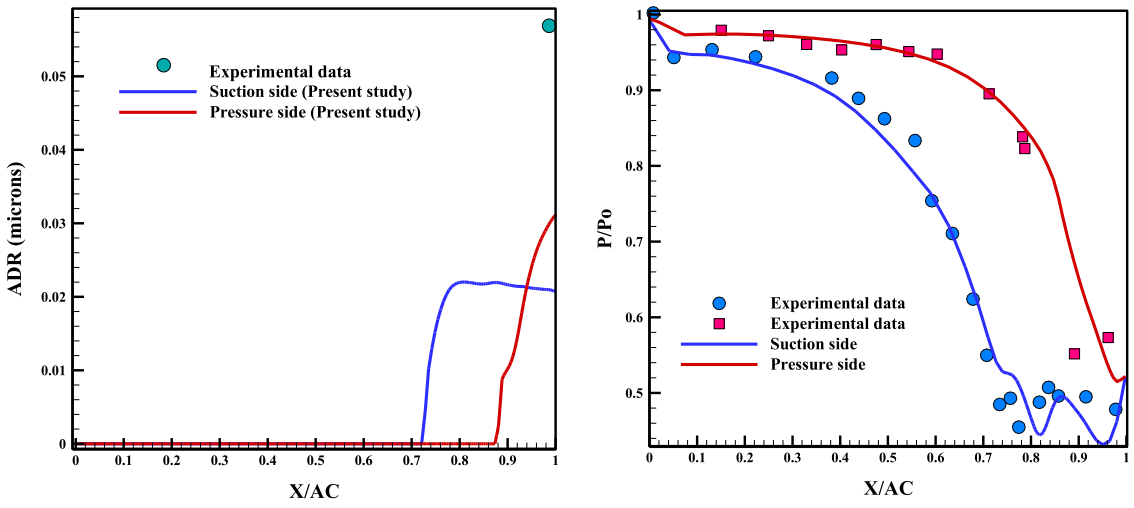

Fig. 5. Comparison of the numerical results of wet steam flow through turbine cascade blades: (a) the average droplet radius and (b) pressure distributions on the suction side, pressure side, and mid passage with experimental data [37].

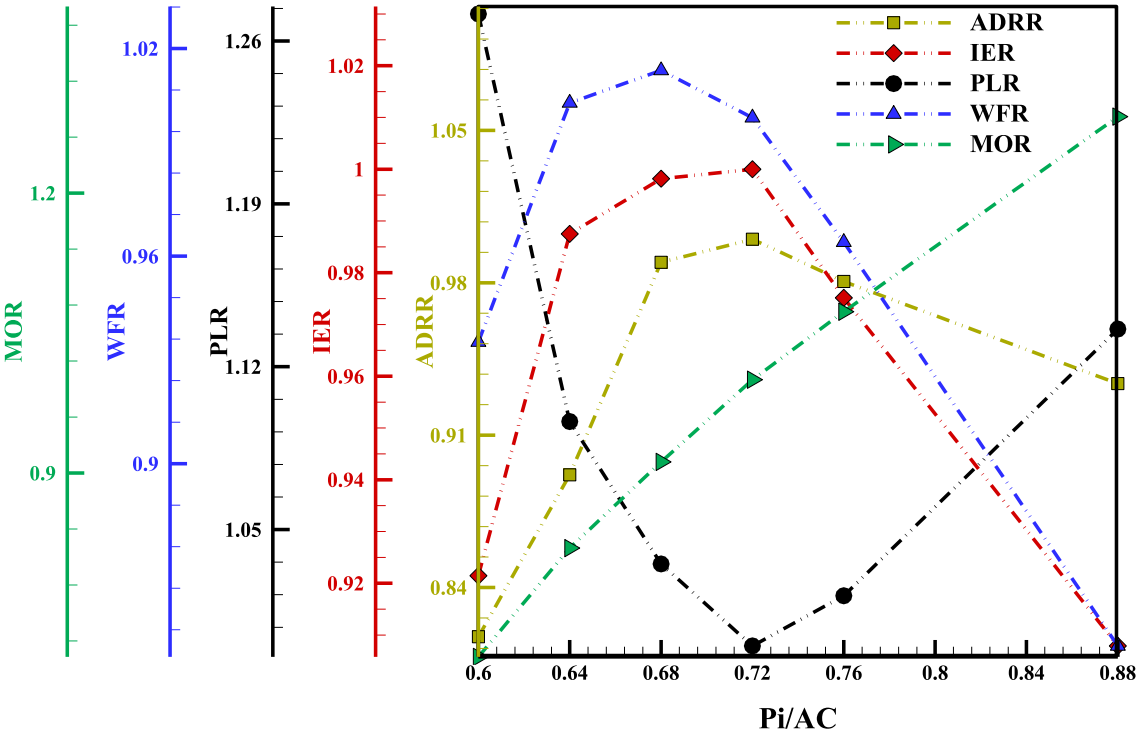

Fig. 6. Effect of pitch variation on the non-dimensional parameters (ADRR: average of droplet radius ratio, IER: isentropic efficiency ratio, PLR: pressure losses ratio, WFR: wetness fraction ratio, MOR: momentum ratio) at the end of the passage.

$$MO = \int_{A2} \rho C^2 dA \tag{36}$$

Dimensionless parameters are utilized in the numerical analysis to show the general trends in the numerical results. Therefore, to make the objective functions of the problem dimensionless, objectives are divided by the original case, as follows:

$$WFR = \frac{WF}{WF_{Original}} \tag{37}$$

$$ADRR = \frac{ADR}{ADR_{Original}} \tag{38}$$

$$PLR = \frac{PL}{PL_{Original}} \tag{39}$$

$$IER = \frac{IE}{IE_{Original}} \tag{40}$$

$$MOR = \frac{MO}{MO_{Original}} \tag{41}$$

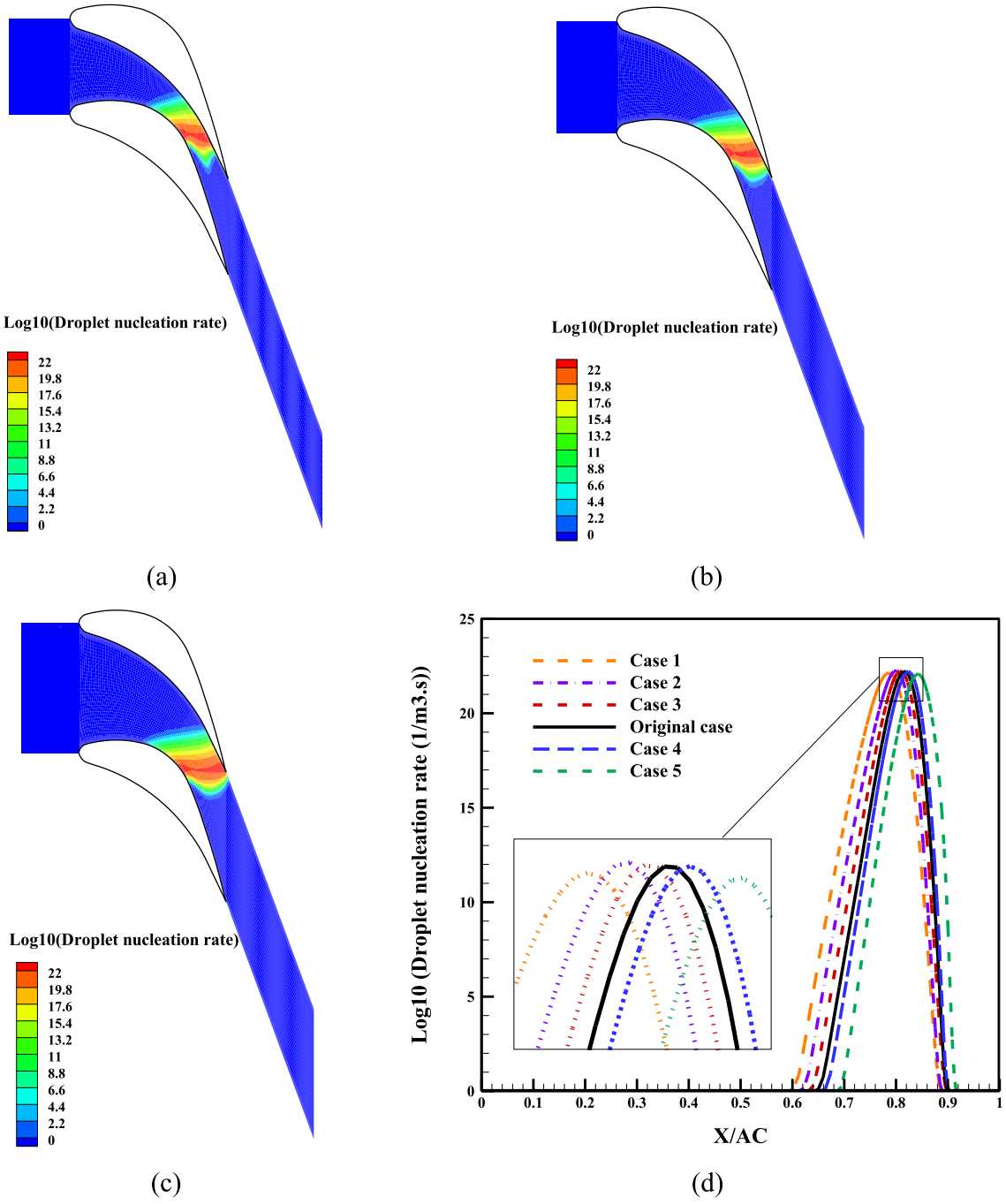

Fig. 7. Effects of pitch variation on the nucleation rate for: (a) case 1, (b) original case, (c) case 5, and (d) on the centerline for different cases.

Table 6
Optimization limits of variables in the present study.

Variables	Upper bound	Lower bound
WFR	1.01	0.84
ADRR	1	0.81
PLR	1.27	1
IER	1	0.90
MOR	1.28	0.70

5. Numerical method

In this study, numerical calculations are performed with compressible and steady-state two-dimensional Reynolds-averaged Navier-Stokes (RANS) equations. The solution methodology of flow solving algorithm was based on an implicit density-based coupled solver. Furthermore, an appropriate description of nucleation and droplet growth is necessary for the analysis of two-phase condensation flow in a cascade turbine blade. Therefore, the Eulerian-Eulerian model is employed for description of two-phase condensation flow in the cascade. The criteria of convergence are below 10^{-6} for all dependent variables.

Table 7
Optimized values of the objective functions (IER, PLR, MOR, ADRR, WFR) and comparison with original case.

WFR	Improved	ADRR	Improved	MOR	Improved	PLR	Degraded	IER	Degraded
0.964	3.59%	0.980	1.94%	1.246	7.28%	1.021	2.15%	0.975	2.48%

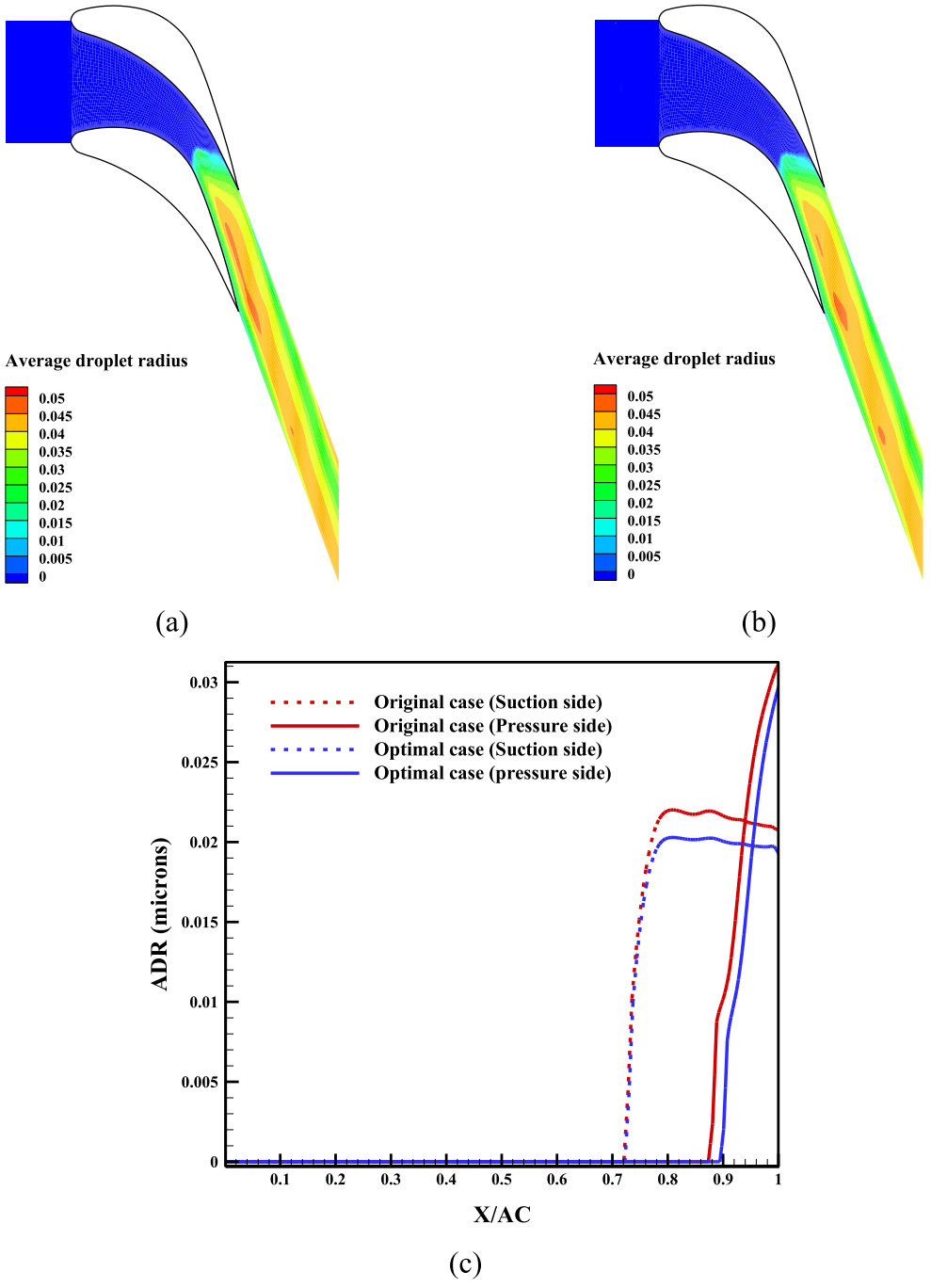

Fig. 8. Effects of the pitch variation on average droplet radius for: (a) original case, (b) optimal case, (c) suction and pressure side for optimal and original cases.

5.1. Grid independence study

To obtain the optimal mesh size, a grid independence study is performed. Fig. 4 indicates the pressure distribution on the suction side through the original blade. Based on Fig. 4, the grid independence is conducted by considering four different grids. According to this figure, the third grid (48*226) indicates condensation shock very well and increasing the density of grids does not change the result. Therefore, the grid with 48 × 226 nodes is obtained as the suitable grid size. In addition, the grid independence for other cases is conducted and tabulated in Table 5.

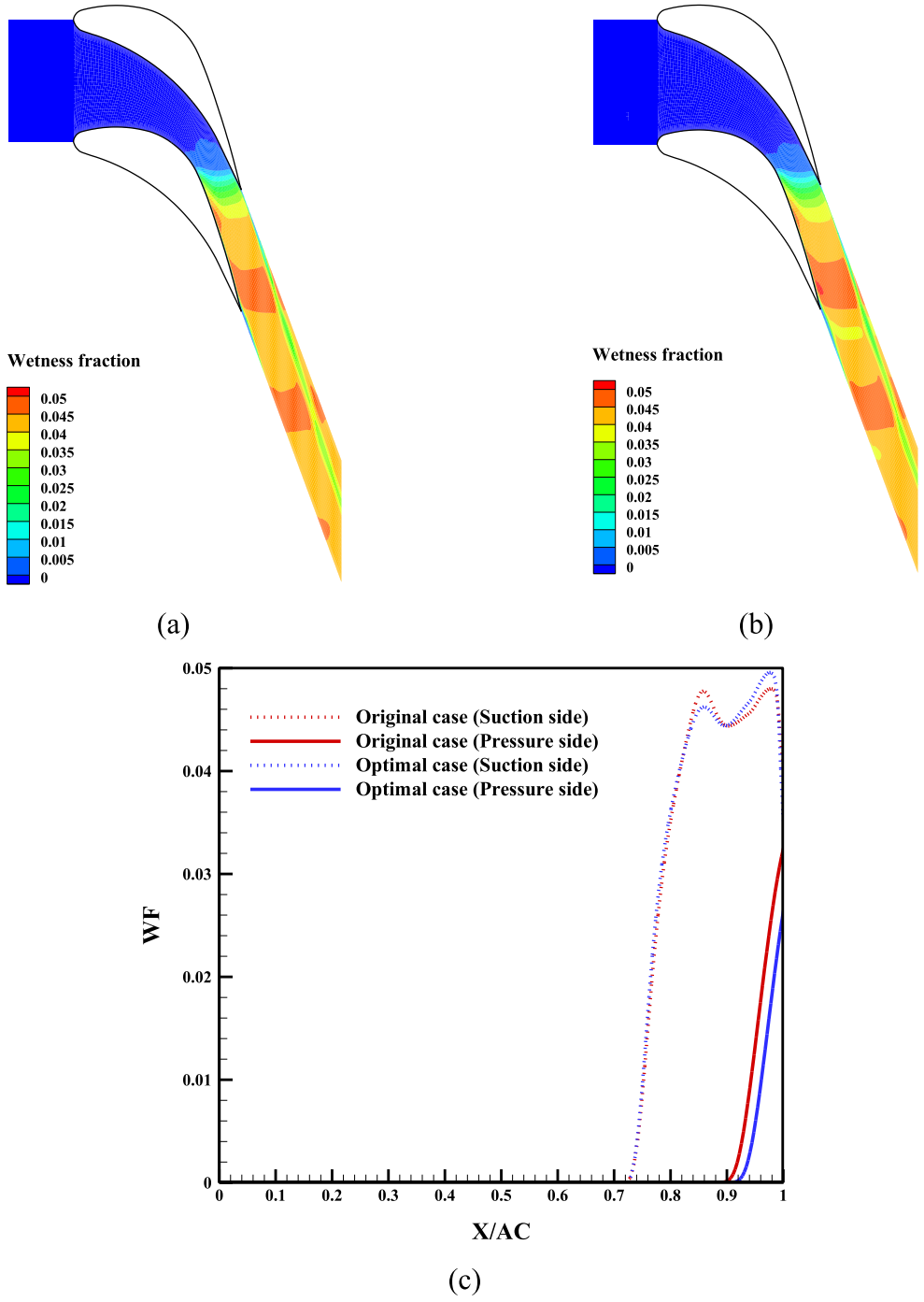

Fig. 9. Effects of the pitch variation on the wetness fraction for: (a) original case, (b) optimal case, (c) suction and pressure side for optimal and original cases.

5.2. Validation

Validation is conducted to confirm the numerical method used in the present study. It is worth mentioning that, Bakhtar et al. [37] in the experimental study, measured the pressure distributions on surfaces and average droplet radius at the end of this blade, respectively. Fig. 5-a, compares the numerical results of average droplet radius on the suction and pressure side with experimental data which is measured at the outlet of the blade. Fig. 5-b, shows the pressure distribution of the numerical and experimental data on the suction and pressure side. It should be noted that the pressure is expanded throughout the passage, until the condensation shock occurs. This shock is beheld as the first pressure rise due to the heat transfer between vapor and droplets. Then pressure reduces until the aerodynamic shock occurs. This shock regulates the pressure in accordance with the back-pressure at the outlet of the blade. The aerodynamic shock is beheld near X/AC = 1 on the pressure side and then reflected on the suction side. The flow is expanded further until the second aerodynamic shock occurs at the outlet of the blade on the suction side. According to the pressure diagram, the pressure on the suction side expands more than pressure side, so nucleation and droplet growth occurs earlier than pressure side. The numerical wet steam results show a good consistency for the pressure distribution and average droplet radius.

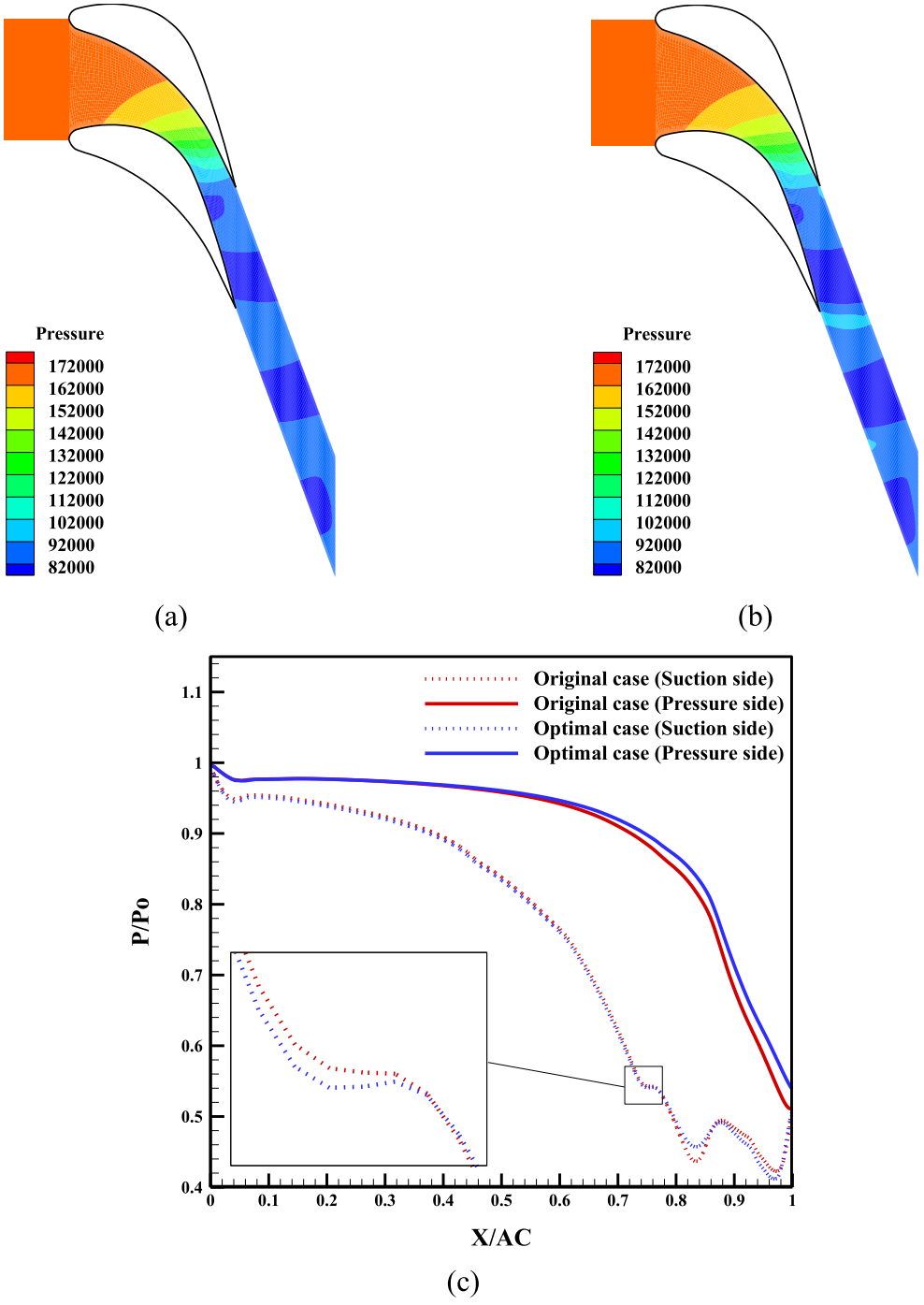

Fig. 10. Effects of the pitch variation on the static pressure for: (a) original case, (b) optimal case, (c) suction and pressure side for optimal and original cases.

6. The effect of pitch variation on wet steam flow

In this study, the effects of variation of pitch to chord ratio on the objective functions are investigated. As already illustrated in Fig. 6, the results of pitch variation on wetness fraction ratio (WFR), average droplets' radius ratio (ADRR), momentum ratio (MOR), pressure loss ratio (PLR), and isentropic efficiency ratio (IER) are provided. Fig. 6 display that the original case (Pi/AC = 0.72) has the most efficiency and the most minor loss.

Based on Eq. (34), the momentum is function of mass flow rate and velocity. Results show that the momentum depend on mass flow rate and velocity has negligible effect on momentum. If the blade pitch increases, more mass flow rate will pass through the passage and consequently the momentum also increases and vice versa. Therefore, the momentum is directly related to the blade pitch to chord ratio.

Wetness fraction depend on average droplet radius and number of droplets. According to Fig. 6, the wetness fraction ratio (WFR) and average droplet radius ratio (ADRR) have same trend except in case (3). The reason is increasing the number of droplets in case (3).

Fig. 7 displays the impact of pitch variation on the nucleation rate. If the blade pitch increases, the expansion rate will decrease and consequently the nucleation rate delays and vice versa. According to Fig. 7, it is clear that with an increase in pitch to chord ratio, nucleation location goes downstream.

7. Optimization results with genetic algorithm

The purpose of this study is to optimize the pitch to chord ratio in which the objective functions included the wetness fraction (WF), average droplet radius (ADR), pressure loss (PL), momentum (MO), and isentropic efficiency (IE); therefore, a genetic algorithm is utilized to optimize the pitch to chord ratio. The upper and lower limits of parameters for this study are provided in Table 6.

After optimization, the genetic algorithm proposed Pi/AC = 0.76. In this case, the Zweifel coefficient is $C_{ZF} = 0.62$. In the other words, Zweifel [28] in an experimental study proposed the optimal ratio of pitch to chord for dry steam turbine blades and the innovation of the present study is the modification of the Zweifel coefficient for wet flow.

Table 7, shows the variation of objective functions. Based on the results, the wetness fraction, average droplet radius, and momentum at the outlet of blade improved 3.59%, 1.94%, and 7.28% respectively. Besides, the isentropic efficiency and pressure loss degraded 2.48% and 2.15%, respectively.

Fig. 8-a-b show the average droplet radius contour in the original case and optimal case, respectively. Moreover, the average droplet radius diagram is provided on the suction side and pressure side in Fig. 8-c for the original case and optimal cases. According to Fig. 7, the nucleation location goes downstream due to increase the pitch to chord ratio, therefore, droplets have less time to grow. It can be inferred from the Fig. 8-c that with an increase one millimeter in blade pitch, droplets generate later. Therefore, droplet radius in the blade outlet is smaller than the original case.

Fig. 9-a-b denote the contour of wetness in the original case and optimal case, respectively. Furthermore, the wetness diagram is provided on the suction side and pressure side (see Fig. 9-c) for the original and the optimal cases. As already shown in Fig. 7, by increasing the blade pitch by one millimeter, nucleation is delayed. On the other hand, according to Fig. 8, droplet radius size is also reduced. Therefore, it is expected that wetness is reduced by increasing the blade pitch.

Fig. 10-a-b demonstrate the pressure contour in the original and the optimal case, respectively. Also, pressure diagram on the suction side, and the pressure side is shown in Fig. 10-c for the original and optimal cases. If the blade pitch increases on millimeter, the expansion rate will decrease and consequently the location of condensation and aerodynamic shocks change.

8. Conclusion

In this paper, the effects of pitch variation on the condensing steam flow parameters are investigated in the stationary cascade of turbine blades. Wetness fraction (WF), average droplet radius (ADR), momentum (MO), pressure loss (PL), and isentropic efficiency (IE) at the outlet are objective functions. The genetic algorithm is utilized to optimize the ratio of pitch to axial chord. Finally, the following results were obtained:

- The optimum pitch to axial chord ratio is obtained (Pi/AC = 0.76).
- In the optimal pitch to axial chord ratio, the Zweifel coefficient is equal to $C_{ZF} = 0.62$.
- In the optimal case, the wetness fraction and the average droplet radius at the outlet decrease 3.59% and 1.94%, respectively, and the momentum increases 7.28%.
- In the optimal case, the isentropic efficiency decreases 2.48%, and the pressure losses increase 2.15%.

Declaration of Competing Interest

The authors declare that they have no known competing financial interests or personal relationships that could have appeared to influence the work reported in this paper.

References

[1] M.T. Somesaraee, E.A. Rad, M.R. Mahpeykar, Analytical investigation of simultaneous effects of convergent section heating of Laval nozzle, steam inlet condition, and nozzle geometry on condensation shock, J. Therm. Anal. Calorim. 133 (2) (2018) 1023–1039, https://doi.org/10.1007/s10973-018-7126-x.

[2] S. Dykas, M. Majkut, M. Strozik, K. Smołka, Experimental study of condensing steam flow in nozzles and linear blade cascade, Int. J. Heat Mass Transf. 80 (2015) 50–57, https://doi.org/10.1016/j.ijheatmasstransfer.2014.09.010.

[3] S. Dykas, M. Majkut, K. Smołka, M. Strozik, Study of the wet steam flow in the blade tip rotor linear blade cascade, Int. J. Heat Mass Transf. 120 (2018) 9–17, https://doi.org/10.1016/j.ijheatmasstransfer.2017.12.022.

[4] D. Walker, S. Barham, D. Giddings, G. Dimitrakis, Wet steam measurement techniques, Rev. Chem. Eng. 35 (5) (2019) 627–647, https://doi.org/10.1515/revce-2017-0078.

[5] J. Joseph, S. Subramanian, K. Vigney, B. Prasad, D. Biswas, Thermodynamic wetness loss calculation in nozzle and turbine cascade: nucleating steam flow, Heat Mass Transf. 54 (8) (2018) 2521–2531, https://doi.org/10.1007/s00231-017-2171-8.

[6] W. Wróblewski, S. Dykas, Two-fluid model with droplet size distribution for condensing steam flows, Energy 106 (2016) 112–120, https://doi.org/10.1016/j.energy.2016.03.052.

[7] L. Cao, J. Wang, H. Luo, H. Si, R. Yang, Distribution of condensation droplets in the last stage of steam turbine under small flow rate condition, Appl. Therm. Eng. 181 (2020) 116021, https://doi.org/10.1016/j.applthermaleng.2020.116021.

[8] B. Sengupta, C. Bhattacharya, Investigation of energy loss on fractional deposition in last stages of condensing steam turbine due to blade shape and moisture droplet size, J. Eng. Gas Turbines Power 140 (7) (2018), https://doi.org/10.1115/1.4038544.

[9] F. Salmani, E. Amiri Rad, M.R. Mahpeykar, Investigation effects of roughness in wet steam flow with Buckingham Pi-theorem, J. Therm. Anal. Calorim. 147 (5) (2022) 3803–3813.

[10] A. Ebrahimi-Fizik, E. Lakzian, A. Hashemian, Entropy generation analysis of wet-steam flow with variation of expansion rate using NURBS-based meshing technique, Int. J. Heat Mass Transf. 139 (Aug. 2019) 399–411, https://doi.org/10.1016/j.ijheatmasstransfer.2019.05.010.

[11] R.A. Alekseev, V.G. Gribin, A.A. Tishchenko, I.Y. Gavrilov, V.A. Tishchenko, V. V. Popov, Investigation of the influence of intra-channel liquid film suction on the structure of the droplet flow downstream a stator blades cascade of a steam turbine, J. Phys. Conf. Ser. 1359 (1) (2019) 12024, https://doi.org/10.1088/1742-6596/1359/1/012024.

[12] A. Ebrahimi-Fizik, E. Lakzian, A. Hashemian, Numerical investigation of wet inflow in steam turbine cascades using NURBS-based mesh generation method, Int. Commun. Heat Mass Transf. 118 (2020) 104812, https://doi.org/10.1016/j.icheatmasstransfer.2020.104812.

[13] H. Ding, Y. Li, E. Lakzian, C. Wen, C. Wang, Entropy generation and exergy destruction in condensing steam flow through turbine blade with surface roughness, Energy Convers. Manag. 196 (2019) 1089–1104, https://doi.org/10.1016/j.enconman.2019.06.066.

[14] G. Zhang, F. Wang, D. Wang, T. Wu, X. Qin, Z. Jin, Numerical study of the dehumidification structure optimization based on the modified model, Energy Convers. Manag. 181 (2019) 159–177, https://doi.org/10.1016/j.enconman.2018.12.001.

[15] M.A.F. Aliabadi, G. Zhang, S. Dykas, H. Li, Control of two-phase heat transfer and condensation loss in turbine blade cascade by injection water droplets, Appl. Therm. Eng. 186 (2021) 116541, https://doi.org/10.1016/j.applthermaleng.2020.116541.

[16] M.A.F. Aliabadi, E. Lakzian, I. Khazaei, A. Jahangiri, A comprehensive investigation of finding the best location for hot steam injection into the wet steam turbine blade cascade, Energy 190 (2020) 116397, https://doi.org/10.1016/j.energy.2019.116397.

[17] M.S. Mirhoseini, M. Boroomand, Multi-objective optimization of hot steam injection variables to control wetness parameters of steam flow within nozzles, Energy 141 (2017) 1027–1037, https://doi.org/10.1016/j.energy.2017.09.138.

[18] M. Vatanmakan, E. Lakzian, M.R. Mahpeykar, Investigating the entropy generation in condensing steam flow in turbine blades with volumetric heating, Energy 147 (2018) 701–714, https://doi.org/10.1016/j.energy.2018.01.097.

[19] R. Hosseini, E. Lakzian, Optimization volumetric heating in condensing steam flow by a novel method, J. Therm. Anal. Calorim. 140 (5) (2020) 2421–2433.

[20] D. Hoseinzade, E. Lakzian, A. Hashemian, A blackbox optimization of volumetric heating rate for reducing the wetness of the steam flow through turbine blades, Energy 220 (2021) 119751, https://doi.org/10.1016/j.energy.2020.119751.

[21] Y. Sui, J. Chen, P. Chu, J. Lan, S. Ren, H. Wu, Y. Xu, J. Xie, J. Ding, Aerodynamic optimization of the last stage turbine blade for an industrial gas turbine, IOP Conf. Ser.: Mater. Sci. Eng. 1081 (1) (2021) 012026.

[22] A. Mahrooghi, E. Lakzian, Optimization of Wells turbine performance using a hybrid artificial neural fuzzy inference system (ANFIS)-Genetic algorithm (GA), Ocean Eng. 226 (2021) 108861, https://doi.org/10.1016/j.oceaneng.2021.108861.

[23] M.A. Trigg, G.R. Tubby, A.G. Sheard, Automatic genetic optimization approach to two-dimensional blade profile design for steam turbines, vol. 121, no. 1, 1999, pp. 11–17. https://doi.org/10.1115/1.2841220.

[24] S.J. Keisari, M. Shams, Shape optimization of nucleating wet-steam flow nozzle, Appl. Therm. Eng. 103 (2016) 812–820, https://doi.org/10.1016/j.applthermaleng.2016.04.134.

[25] C. Wen, Y. Yang, H. Ding, C. Sun, Y. Yan, Wet steam flow and condensation loss in turbine blade cascades, Appl. Therm. Eng. 189 (2021) 116748, https://doi.org/10.1016/j.applthermaleng.2021.116748.
[26] S.M.A.N.R. Abadi, A. Ahmadpour, S. Abadi, J.P. Meyer, CFD-based shape optimization of steam turbine blade cascade in transonic two phase flows, Appl. Therm. Eng. 112 (2017) 1575–1589, https://doi.org/10.1016/j.applthermaleng.2016.10.058.
[27] X. Han, W. Zeng, Z. Han, Numerical investigation of the condensation flow characteristics and modification optimization of a condensing steam turbine cascade, Int. J. Numer. Meth. Heat Fluid Flow 29 (2019) 4531–4548, https://doi.org/10.1108/HFF-03-2019-0269.
[28] O. Zweifel, Optimum Blade Pitch for Turbo-Machines with Special Reference to Blades of Great Curvature, Eng. Dig. 7 (11) (1946) 358–360.
[29] V. Dossena, G. D'Ippolito, E. Pesatori, Stagger angle and pitch-chord ratio effects on secondary flows downstream of a turbine cascade at several off-design conditions, Turbo Expo: Power for Land, Sea, and Air 41707 (2004) 1429–1437, https://doi.org/10.1115/GT2004-54083.
[30] P.J. Walker, J.A. Hesketh, Design of low-reaction steam turbine blades, Proc. Inst. Mech. Eng. Part C J. Mech. Eng. Sci. 213 (2) (1998) 157–171, https://doi.org/10.1243/0954406991522248.
[31] K. Segawa, Y. Shikano, T. Takano, A high performance optimized reaction blade for high pressure steam turbines, Mar. 30, 2004, pp. 307–314. https://doi.org/10.1115/POWER2004-52110.
[32] K. Segawa, Y. Shikano, K. Tsubouchi, N. Shibashita, Development of a highly loaded rotor blade for steam turbines (2nd Report, three-dimensional stage performance verifications), JSME Int. J. Ser. B Fluids Therm. Eng. 45 (4) (2002) 881–890, https://doi.org/10.1299/jsmeb.45.881.
[33] L. Teia, New supersonic loss model for the preliminary design of transonic turbine blades and the influence of pitch, J. Turbomach. 142 (4) (2020) 41008, https://doi.org/10.1115/1.4045983.
[34] M. Mesbah, V.G. Gribin, K. Souri, Investigation of the effects of main geometric parameters and flow characteristics on secondary flow losses in a turbine cascade, J. Phys. Conf. Ser. 2131 (3) (2021) 32081, https://doi.org/10.1088/1742-6596/2131/3/032081.
[35] E. Flídr, T. Jelínek, M. Kladrubský, Experimental Investigation of Effects of Reynolds Number and Incidence Angle on Secondary Flow within a Linear Blade Cascade, J. Therm. Sci. 30 (6) (2021) 2122–2136, https://doi.org/10.1007/s11630-021-1455-y.
[36] D. Lengani, D. Simoni, V. Yepmo, M. Ubaldi, P. Zunino, F. Bertini, Low rank education of cascade loss sensitivity to unsteady parameters by Proper Orthogonal Decomposition, J. Turbomach. 143 (11) (2021), https://doi.org/10.1115/1.4051273.
[37] F. Bakhtar, M.R. Mahpeykar, K.K. Abbas, An Investigation of Nucleating Flows of Steam in a Cascade of Turbine Blading-Theoretical Treatment This, J. Fluids Eng. 117 (1) (1995) 138–144.
[38] A. Hashemian, E. Lakzian, A. Ebrahimi-Fizik, On the application of isogeometric finite volume method in numerical analysis of wet-steam flow through turbine cascades, Comput. Math. Appl. 79 (6) (2020) 1687–1705, https://doi.org/10.1016/j.camwa.2019.09.025.
[39] M.J. Kermani, A.G. Gerber, A general formula for the evaluation of thermodynamic and aerodynamic losses in nucleating steam flow, Int. J. Heat Mass Transf. 46 (17) (2003) 3265–3278, https://doi.org/10.1016/S0017-9310(03)00096-6.
[40] Y. Patel, G. Patel, T. Turunen-Saaresti, Influence of turbulence modelling on non-equilibrium condensing flows in nozzle and turbine cascade, Int. J. Heat Mass Transf. 88 (2015) 165–180, https://doi.org/10.1016/j.ijheatmasstransfer.2015.04.069.
[41] X.-D. Wang, J.-L. Dong, T. Wang, J.-Y. Tu, Numerical analysis of spontaneously condensing phenomena in nozzle of steam-jet vacuum pump, Vacuum 86 (7) (2012) 861–866, https://doi.org/10.1016/j.vacuum.2011.02.016.
[42] K. Ishizaka, A high-resolution numerical method for transonic non-equilibrium condensation flow through a steam turbine cascade, Proc. 6th ISCFD 1 (1995) 479–484.
[43] A.M. Dolatabadi, E. Lakzian, M. Heydari, A. Khan, A modified model of the suction technique of wetness reducing in wet steam flow considering power-saving, Energy 238 (2022) 121685.
[44] F. Bakhtar, M.Y. Zamri, J.M. Rodriguez-Lelis, A comparative study of treatment of two-dimensional two-phase flows of steam by a Runge-Kutta and by Denton's methods, Proc. Inst. Mech. Eng. Part C J. Mech. Eng. Sci. 221 (6) (2007) 689–706, https://doi.org/10.1243/0954406JMES477.
[45] F. Bakhtar, M. Ebrahimi, R.A. Webb, On the performance of a cascade of turbine rotor tip section blading in nucleating steam: part 1: surface pressure distributions, Proc. Inst. Mech. Eng. Part C J. Mech. Eng. Sci. 209 (2) (1995) 115–124, https://doi.org/10.1243/PIME_PROC_1995_209_131_02.
[46] J.B. Young, An Equation of State for Steam for Turbomachinery and Other Flow Calculations, J. Eng. Gas Turbines Power 110 (1) (1988) 1–7, https://doi.org/10.1115/1.3240080.
[47] F.R. Menter, Two-equation eddy-viscosity turbulence models for engineering applications, AIAA J. 32 (8) (1994) 1598–1605, https://doi.org/10.2514/3.12149.
[48] A. Ebrahimi-Moghadam, S. Kowsari, F. Farhadi, M. Deymi-Dashtebayaz, Thermohydraulic sensitivity analysis and multi-objective optimization of Fe3O4/H2O nanofluid flow inside U-bend heat exchangers with longitudinal strip inserts, Appl. Therm. Eng. 164 (2020) 114518, https://doi.org/10.1016/j.applthermaleng.2019.114518.
[49] S. Kowsari, M. Deymi-Dashtebayaz, K. Karbasi, H. Sheikhani, Optimal working conditions of various city gate stations for power and hydrogen production based on energy and eco-exergy analysis, Int. J. Hydrogen Energy 45 (43) (2020) 22513–22533, https://doi.org/10.1016/j.ijhydene.2020.05.110.
[50] D. Hoseinzade, E. Lakzian, S. Dykas, Optimization of the Trailing Edge Inclination of Wet Steam Turbine, vol. The Societ, 2021. https://doi.org/10.1007/s40799-021-00534-5.
[51] S. M. Yahya, Turbines, Compressors and Fans 2nd ed., Tata McGraw-Hill Publishing Company Limited, 2002 (Online). Available: https://books.google.com/books?id=mYeNd_jnMvkC&pgis=1.